

# Excitation and relaxation dynamics in ultrafast laser irradiated optical glasses

C. Mauclair<sup>1</sup>, A. Mermillod-Blondin<sup>2</sup>, K. Mishchik<sup>1</sup>, J. Bonse<sup>3</sup>, A. Rosenfeld<sup>2</sup>, J. P. Colombier<sup>1</sup>, and R. Stoian<sup>1</sup>

<sup>1</sup>Laboratoire Hubert Curien, UMR 5516 CNRS, Université de Lyon, Université Jean Monnet, 42000 Saint Etienne, France

<sup>2</sup>Max-Born-Institut für Nichtlineare Optik und Kurzzeitspektroskopie, 12489 Berlin, Germany

<sup>3</sup>Bundesanstalt für Materialforschung und -prüfung (BAM), 12205 Berlin, Germany

(Received 8 July 2016; revised 22 September 2016; accepted 25 October 2016)

## Abstract

We discuss the dynamics of ultrashort pulsed laser excitation in bulk optical silica-based glasses (fused silica and borosilicate BK7) well-above the permanent modification threshold. We indicate subsequent structural and thermomechanical energy relaxation paths that translate into positive and negative refractive index changes, compression and rarefaction zones. If fast electronic decay occurs at low excitation levels in fused silica via self-trapping of excitons, for carrier densities in the vicinity of the critical value at the incident wavelength, persistent long-living absorptive states indicate the achievement of low viscosity matter states manifesting pressure relaxation, rarefaction, void opening and compaction in the neighboring domains. An intermediate ps-long excited carrier dynamics is observed for BK7 in the range corresponding to structural expansion and rarefaction. The amount of excitation and the strength of the subsequent hydrodynamic evolution is critically dependent on the pulse time envelope, indicative of potential optimization schemes.

**Keywords:** carrier plasmas; glasses; pulse shaping; refractive index engineering; ultrafast laser excitation

## 1. Introduction

Laser-induced three-dimensional transformation of bulk transparent materials carries today a strong potential in photonic technologies. This concerns the accurate design of the dielectric function via local laser-induced refractive index changes, serving in the fabrication of embedded optical components in fibers and bulk materials<sup>[1]</sup>. Laser-induced phenomena can equally affect the resistance of optical materials to damage and breakdown, posing severe limitations to high power laser installations, fiber communication setups, or optical control elements in harsh environments<sup>[2]</sup>. These elements justify the strong interest in the fundamentals of laser-induced electronic and structural modifications of transparent materials on macro-, micro- and mesoscopic scales. Particularly, ultrafast laser radiation can strongly localize excitation in space and time, determining in turn a range of phenomena: from electronic runaway or transient defects states to macroscopic thermomechanical phenomena<sup>[3, 4]</sup>. All these processes are mediated by the behavior of laser-induced electronic excitation. Its evolution

is therefore of interest. In fused silica, a material of technological interest and thoroughly investigated, several particular physical manifestations were observed. Saeta *et al.*<sup>[5]</sup> and Audebert *et al.*<sup>[6]</sup> indicated more than a decade ago a characteristic fast sub-ps relaxation channel for excited carriers in self-induced lattice distortions with the formation of self-trapped excitonic (STE) states and their conversion to Frenkel pairs (nonbridging oxygen and  $E'$  centers). This is indicative for a still rigid matrix, whereas as the level of excitation increases, the relaxation times become long, suggesting a decrease in the trapping capacity, consequence of vibrational molecular activity in low viscosity phases<sup>[7]</sup>.

A range of techniques were developed to observe the dynamics of electron-hole pairs in various dielectrics, ranging from phase-sensitive interferometry and transient absorption spectroscopy to time-domain THz spectroscopy or imaging and digital holography. Thus information on real and imaginary parts of the transient dielectric function were mapped in space and time, identifying relaxation states or damage dynamics<sup>[8–12]</sup>. These are essential not only for determining the nature of laser-induced transformations but also for getting further access to the energy balance of the process and for elucidating paramount nonlinear propagation effects assisting the energy deposition. The excited

Correspondence to: R. Stoian, Laboratoire Hubert Curien, UMR 5516 CNRS, Université de Lyon, Université Jean Monnet, 18 Rue Benoit Lauras, 42000 Saint Etienne, France. Email: [razvan.stoian@univ-st-etienne.fr](mailto:razvan.stoian@univ-st-etienne.fr)

dielectrics follow short- and long-living absorption phases, associated to carrier dynamics in strong or weak interaction with the glass matrix<sup>[7, 13–15]</sup>. The material structurally responds to this dynamics on various timescales with structural states ranging from densification (type I) to rarefaction (type II)<sup>[16–19]</sup>. The thermodynamic relaxation behavior and the structural metastability, strongly glass-dependent, are playing an important role<sup>[20]</sup>. This is evident in comparing fused silica and borosilicate glasses with different glass transition behaviors. The latter glass type, still relying on a silica matrix, shows the influence of different expansion coefficient, softening temperature, and Young modulus<sup>[18]</sup>. The different relaxation dynamics can then be exploited using pulse shaping techniques in the time domain. These are capable of adjusting the energy delivery rate to the transient change of material states<sup>[15]</sup>, thus reinforcing the efficiency of energy deposition.

We report here a space and time-resolved investigation of the dynamics of single Gaussian ultrashort laser pulse excitation and energy relaxation in two model materials: amorphous fused silica (a-SiO<sub>2</sub>) and borosilicate crown glass (BK7), exhibiting different optical and thermomechanical properties. The irradiation characteristics correspond mostly to type II regimes above the threshold for void formation, in conditions of moderate focusing. Employing optical transmission microscopy (OTM) and phase-contrast microscopy (PCM) we discuss dose-dependent electronic relaxation times and their consequence in permanent damage morphologies. The follow-up characteristic dynamics of the glass matrix, the subsequent geometry and evolution of the heat source, down to the formation of pressure waves are indicated. The role of pulse duration in stepwise controlling and maximizing energy deposition and confinement is pointed out, suggesting optimization schemes and conditions.

## 2. Methods

### 2.1. Experimental arrangement and data analysis

Parallelepipedic a-SiO<sub>2</sub> and BK7 samples polished on all faces were irradiated with pulses originating from an ultrafast laser system delivering ultrashort pulses (120 fs) at 800 nm central wavelength and an effective repetition rate of 2 Hz. The samples are mounted on an XYZ precision positioning system and placed under in situ microscopic observation, with details given in Ref. [21]. The laser beam is divided in two parts, one (pump) preserved at the fundamental wavelength is employed to excite the material, while the second (probe) is frequency doubled (400 nm) and used to image the excitation region in a perpendicular side-geometry at different time moments after excitation. A temporal resolution better than 0.6 ps is ensured for the time-synchronization of the two beams via an optical delay

line. A microscope objective (numerical aperture  $NA = 0.45$ ) focuses the pump beam inside the glass sample. The effective numerical aperture is determined by beam truncation at  $NA = 0.3$ . The focal plane is fixed in the bulk at a distance of 200  $\mu\text{m}$  from the surface, minimizing the wavefront distortions generated at the interface. The blue probe beam enters the illumination path of a positive phase-contrast microscope (Olympus BX41) in Köhler geometry. This setup allows for ultrafast imaging in OTM or PCM mode<sup>[21]</sup>. In the OTM mode the absorption region appears darker on the illumination background, marking a decrease in transmission, whereas in PCM mode relative negative (positive) index changes are appearing light (dark) on a dark background. The image is recorded with a back-illuminated electron multiplier CCD camera. A bandpass filter at 400 nm rejects parasitic light emitted by the irradiated specimen and scattered pump light. The onset of the pump-induced free carrier absorption is used to define the temporal synchronization between excitation and detection. Speckle noise generated by the employment of imaging optics and light homogenizing scattering plates in the probe beam path was reduced by rotating the plates and accumulating  $N_i$  images of the same event. In OTM, we chose  $N_i = 50$  and in PCM,  $N_i = 100$ . The sample was translated after each laser shot to ensure for fresh excitation regions.

A data processing formalism was used to extract quantitative information concerning laser-excited free carriers. The OTM images realized perpendicular to the object axis represent a projection of the absorptive properties of the electron gas, giving thus the integrated absorbance along the probing path. They deliver a first glance into the potential electronic densities and their dynamics<sup>[12]</sup>. Within the hypothesis that the excitation object is axially symmetric along the pulse propagation axis, a reverse Abel transform is performed to extract the local absorption coefficient. Using a Drude model for the laser-induced carrier plasma, the variation of the extinction coefficient is  $\Delta k_e = -n_0 N_e / 2N_c \omega \tau / [1 + (\omega \tau)^2]$ , with  $N_c$  being the critical density (in the range of  $10^{21} - 10^{22} \text{ cm}^{-3}$  at 800 nm), where the real part of the complex permittivity  $\Re[\epsilon^*] = 0$ . The analysis takes into account the specific illumination wavelength. The detected values are strongly dependent on the considered parameters, namely the carrier momentum scattering time ( $\tau$ ), which is fixed here at 0.5 fs<sup>[7]</sup>, and the electronic mass, implicitly considered via normalization to the critical density in the bulk. This represents a strong approximation as in dense electron-hole carrier systems in ionized solids the collision frequency for electronic collision events (capable of modifying the overall momentum and thus generating an absorption step) may easily vary between  $10^{15}$  and  $10^{16}$  Hz depending on density and the energy distribution of the carriers, and the energy band structure of the host matrix. In this respect the detected electronic values should be considered with precaution and will mainly serve for comparative purposes between various relaxation conditions.

Post-irradiation microscopy and site-specific photoluminescence spectroscopy mapping (under HeCd laser excitation at 325 nm wavelength) were carried out on the laser-induced damage traces to observe subsequent permanent changes in the electronic structure.

### 3. Results and discussion

#### 3.1. Time-resolved investigations of carrier dynamics in fused silica glass

The nature and the morphological aspect of optical damage, namely the potential onset of refractive index changes, regular voids or catastrophic runaway is strongly dependent on the deposited energy. The low exposure domain, at pump energies below or close to observable modifications, was regularly investigated and indicates fast relaxation (100 fs) and trapping of free carriers on excitonic states self-trapped due to the electronic polarization of the matrix. These evolve to Frenkel pairs and the Si–O bond scission leads to nonbridging oxygen hole center (NBOHC) and  $E'$  centers accompanying a soft isotropic increase of the refractive index upon pulse accumulation. It was argued before<sup>[7, 22]</sup> that, most probably, the weak positive index changes regime results from defect-induced matrix densification without visible thermal assistance in driving the structural metastability. Photoinscription in this range leads to type I index changes and low-loss waveguides<sup>[1]</sup>. Increasing the incoming laser pulse energy above the critical power for self-focusing (corresponding to sub- $\mu\text{J}$  ranges), the morphology of the excited region changes to a modulated positive and negative index region. A detailed description of the nonlinear propagation factors leading to this geometry was given in Ref. [23]. The onset of the formation of void-like low index regions can be assigned to self-focusing and expansion, while the follow-up positive index trail indicates filamentation characteristics<sup>[23, 24]</sup>. Both regions are permanently visible after single-shot interaction. If low-density regions can originate from thermomechanical expansion, the void formation is usually assigned to a microexplosion phenomenon<sup>[25]</sup> being driven by high pressure, high temperature material states against the mechanical resistance of the surrounding cold material. Beyond this, at high input energies, a catastrophic, stochastic-like damage occurs comprising multiple voids and index regions of different contrasts. This signals strongly unstable propagation with multiple points of energy concentration where thermodynamic conditions for void expansion and stress development are achieved. We concentrate here on energetic conditions in the catastrophic regime as it allows to study the relaxation behavior in strong excitation conditions at the focus and in low excitation conditions at the neighboring regions in the spatial distribution of the incoming Gaussian pulse.

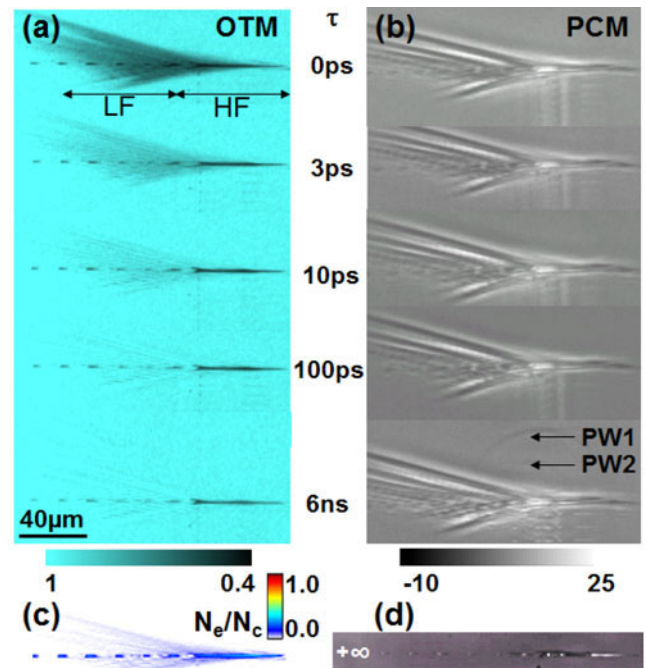


**Figure 1.** Time-resolved observation of laser excitation and subsequent relaxation in fused silica in (a) OTM and (b) PCM modes at energies significantly above the void-formation threshold (high-energy range). Input energy  $E = 43 \mu\text{J}$  and pulse duration  $t_p = 160 \text{ fs}$ . Two characteristic regions in terms of dynamics are indicated as LF region and HF region. (c) Estimated maximum electronic density at zero delay, at the excitation peak. (d) PCM aspect of the permanent damage. Transmission and relative phase change scale bars are given, as well as normalized (to critical density at 800 nm) scales for carrier density. The laser pulse is coming from the left.

The first set of high-energy time and space-resolved excitation snapshots in a-SiO<sub>2</sub> are given in Figure 1 in terms of transient OTM images [Figure 1(a)], PCM images [Figure 1(b,d)] and Drude-based carrier densities [Figure 1(c)]. The input energy of  $E = 43 \mu\text{J}$  is well-above the threshold for the void formation (around 0.23  $\mu\text{J}$ ). The transmission signatures are determinantly originating in the development of free carriers and reflect mainly the properties of a collisional electron–hole plasma but they may equally involve mobile excitonic states bordering the allowed energy bands. With reference to the OTM micrographs, characteristic to this figure is the existence of two spatially distinct regions with two characteristic dynamics. The low fluence (LF) region located before the pulse concentration at the focus [Figure 1(a)] is subject to low-energy concentration while a high fluence (HE) region is located along the confocal domain and corresponds to the maximal energy concentration (corresponding to fluences above 1000  $\text{J}/\text{cm}^2$  in vacuum). Given the light defocusing strength of self-induced carriers, the local fluences in the bulk are significantly lower. They preserve nevertheless considerable values, above the material destruction point. The multiple points before the focus are an effect of diffraction at the objective aperture and scattering of wavefronts toward the propagation axis<sup>[26]</sup>.

The LF region [Figure 1(a)] shows a fast evolution of OTM with a rapid recovery. This corresponds to a fast electronic decay with a sub-ps decay constant. This rapid characteristic dynamics is the signature of a carrier trapping mechanism where free carriers are trapped into immobile excitonic states<sup>[6]</sup> associated with localized structural changes. Evidence of NBOHC was found in this regime<sup>[7, 22, 27]</sup> with signs of structural compaction. This is equally a typical material modification regime in terms of photon doses for the photoinscription of soft, low contrast refractive index changes, also obtained in intensity clamping conditions. Complementary PCM shows the variation of the optical phase deriving from a mix of electronic and structural effects. We suggest that the latter are preponderant in view of the rapid electronic decay. The comparative observation of PCM images [Figure 1(b)] with their representation of the acquired optical phase shows that associated structural modifications start almost simultaneously with electronic excitation, suggesting a rapid response to electronic excitation. The dark regions correspond to a fast (and transient) index increase (the residual white may be an artefact of PCM at high index contrast). However, this structural perturbation initiated by electronic excitation within the LF region has a significantly longer lifetime than the carrier plasma and survives up to ns ranges. This transient phase shift can then be put in relation to the characteristic structural and electronic local rearrangement related to STE evolution (displacement of oxygen atoms and the onset of excitonic localized bands in the forbidden gap)<sup>[6, 7]</sup>. Si–O molecular bonding is loosening and a more compacted structural arrangement (lower size rings) can be obtained in the fused silica matrix. Due to its fast onset, the phase dynamics seems less related to local heating but heat contributions cannot be excluded. The typical level of excitation in this range is a fraction of the critical density at 800 nm [Figure 1(c)]. It is though to be noted that for a glass with a positive thermo-optic coefficient, a fast increase of temperature would equally lead to a positive index change.

The OTM dynamics in the HF region is different, as the increase of the incoming fluence delivers a radically distinct behavior in terms of relaxation times [Figure 1(a)]. As opposed to what is typically seen for the low dose regime, we note now a persistent long-living high level of absorption (tens of percent) and consequently, a relatively long relaxation time for the axial region (on hundreds of ps, up to the ns). The long-living absorption trail is no longer consistent with fast trapping mechanisms via deformation potentials, suggesting a matrix structural state unable to trap carriers. This may be indicative of strongly destabilized molecular bonds or of a rapid onset of a low viscosity state with vibrational activity. The corresponding PCM observations seem to confirm the existing and long-living electron plasma on longer timescales, although the interpretation is more difficult due to the mixed amplitude and phase properties of

the object and the plasma radiative emission. An estimation of the carrier density at the peak of the laser pulse leads to values close to the critical density at 800 nm. It is though to be noted that, in view of the collisional properties of the plasma (sub-fs collision times) which give a strongly dissipative character, no sharp resonance is to be expected at the critical density, and therefore the use of a critical density is just indicative but without the relevance of a sudden absorptive regime. Carrier densities in this range are sufficient to rise the matrix temperature after relaxation at considerable temperature values.

The permanent damage morphology visible in Figure 1(d) consists of a more or less random succession of void-like and high index zones only in the confocal domain in the high excitation range, the changes in the perifocal range being too weak to be observed in a single-shot event. It is therefore expectable that this characteristic morphology modification involves transitions via lower viscosity states (even though perhaps not yet a fully developed liquid phase) and the onset of the void is a result of the mechanically induced rarefaction<sup>[24, 25]</sup>. Photoluminescence signatures indicated the presence of oxygen deficiency centers (ODC) in the vicinity of the void interfaces and the onset of molecular oxygen<sup>[22]</sup>. These support present scenarios of molecular decomposition that assume that enough energy is provided to the glass matrix to facilitate the onset of gas-phase transformation in void-like domains<sup>[20, 28]</sup>. The absence of strong NBOHC yield in the regions of the catastrophic damage<sup>[22]</sup> corroborated with the long dynamics of the relaxation times seems to confirm a significant decrease of the electron trapping strength, as matrix heating or vibrational activity associated to lower viscosity kicks in and lowers the molecular polarization potential. Alternative pathways of structural reorganization of the matrix in the presence of significant bond-breaking, favored by excessive heat and pressure, may contribute to the absence of NBOHC. A sketch of defect redistribution in the high-energy damage area<sup>[22, 29]</sup> is given in Figure 2. The photoluminescence spectrum is taken under conditions of excitation at 325 nm, resonant with NBOHC states. This observation shows that the rapid relaxation domain at low doses is the preferential region for forming NBOHCs, a natural product of electron trapping and STE relaxation, while the axial damage shows molecular decomposition and sever bond-breaking regime with ODC formation. Similar defect signatures appear equally in neighboring zones subjected to thermomechanical transformation but less to light exposure. This suggests a competition of electronic and mechanical bond-breaking effects above plastic yielding.

To resume, we have observed in fused silica two characteristic fast and slow electron dynamics ranges characterized by rather low or high carrier densities that translate into specific damage aspects culminating with catastrophic runaway and stochastic void formation. This shows the pertinence of considering high- and low-energy density deposition domains, as paths of structural relaxation will be different.

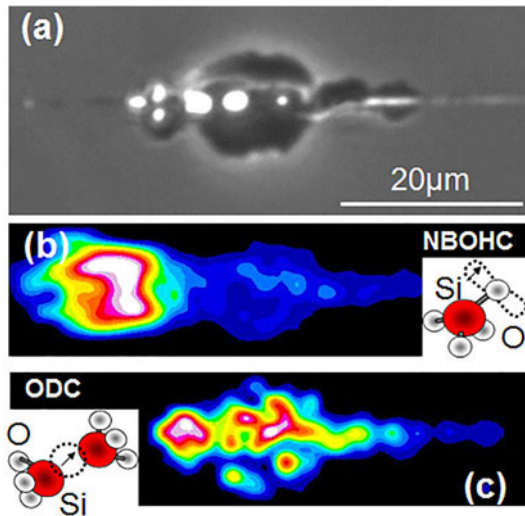


**Figure 2.** Post-irradiation PCM and photoluminescence spectroscopy analysis in the fast and slow decay zones for a typical trace in the high-energy interaction domain<sup>[29]</sup>. (a) PCM of the modification region with the appearance of voids in the long-living excitation zone. (b) Generation of NBOHC in the soft, fast decay region, visualized by spatially mapping photoluminescence centered at 650 nm. (c) Accumulation of ODC in permanent void-like damage regions, with photoluminescence bands centered at 545 nm. A 325 nm excitation source is used.

### 3.2. Time-resolved investigations of carrier dynamics in borosilicate BK7 glass

Since fused silica is a glass with an atypical thermodynamic behavior (various anomalies in glass transition and in the thermomechanical evolution) and relatively low thermal expansion, it is interesting to perform a similar experiment of a different class of silicate glasses with a more common behavior [with results given in Figure 3]. We have chosen a borosilicate crown glass, the Schott BK7, a glass relying on silica and boric oxide as glass formers and light metallic impurities, but showing normal glass transition behavior. This implies that, upon cooling to the glassy state, the material density increases with the cooling time. Moreover, BK7 shows an approximately ten times higher thermal expansion coefficient facilitating expansion upon heating in the glassy state.

Figures 3(a) and 3(b) shows the electronic relaxation and the corresponding optical response for high-energy excitation of BK7 (43  $\mu$ J). As in the case of fused silica, two regions can be discerned. In the LF region, the electronic density decays gradually with a characteristic time that exceeds 10 ps. Slightly shorter times (8 ps) were obtained at lower dose<sup>[30]</sup>, still significantly higher than what is expected for a-SiO<sub>2</sub>. The PCM optical shift shows that a transient structural destabilization follows the electronic excitation and survives the electronic decay to longer times. In the HF region, the decay time seems even longer, and the electronic contribution appears visible in both OTM and PCM. The peak electronic density [Figure 3(c)] that triggered this

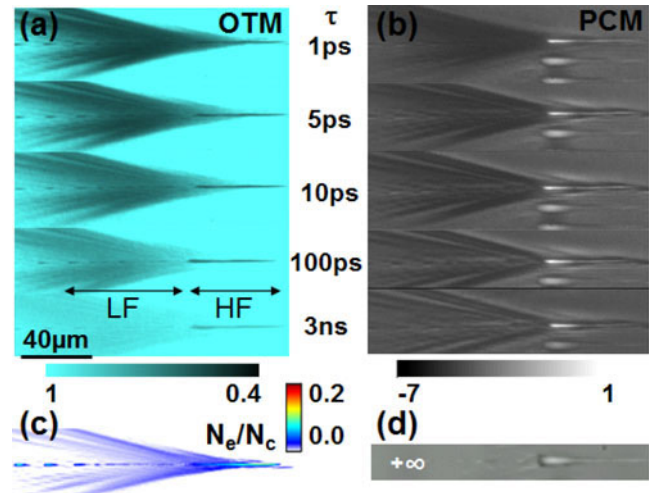


**Figure 3.** Time-resolved observation of excitation and relaxation in borosilicate BK7 in (a) OTM and (b) PCM modes at energies significantly above the void-formation threshold (high-energy range). Input energy  $E = 43 \mu\text{J}$  and pulse duration  $t_p = 160 \text{ fs}$ . Two characteristic regions in terms of dynamics are indicated as LF region and HF region. (c) Estimated peak electronic density at zero delay. (d) PCM aspect of the permanent damage. Transmission and relative phase change scale bars are given, as well as normalized (to critical density at 800 nm) scales for carrier density. The laser pulse is coming from the left.

behavior is in the same order of magnitude, though somehow smaller, as for fused silica, despite a narrower band gap and an a priori higher excitation efficiency. This is intrinsically related to a certain light-scattering role of the free carriers, resisting thus to energy deposition.

In the energy range involved here, the permanent result of laser irradiation in BK7 in terms of damage appearance is a large, elongated, quasi-uniform region of negative refractive index change surrounded by a shallow layer of compressed material and low index features before the confocal region. Thus a rarefaction type of response is observed at the level of the glass matrix. It is conceivable that this corresponds to a local thermal expansion phenomenon leaving behind a low-density region<sup>[18]</sup>.

We note that the observed dynamics for fused silica and borosilicate BK7 are quite general, irrespective of the input energy in the domain where catastrophic damage is achieved. The whole spatially and temporally resolved dynamics for a moderate energy is given in Figure 4 as OTM and PCM results, illustrating the existence of two characteristic dynamic behaviors for low and respectively high levels of excitation. Similar electronic and structural observations from OTM and PCM can be drawn, with fast carrier decay in LF-like regions (sub-ps for fused silica and few ps for BK7), but persisting structural signatures, and slow decay of carriers in HF-like domains. Thus the different relaxation dynamics suggests either soft or severe, thermally mediated structural changes. The difference in the relaxation speed for a-SiO<sub>2</sub> (sub-ps) and BK7 (ps) in the fast dynamics range (LF) suggest nevertheless a qualitative

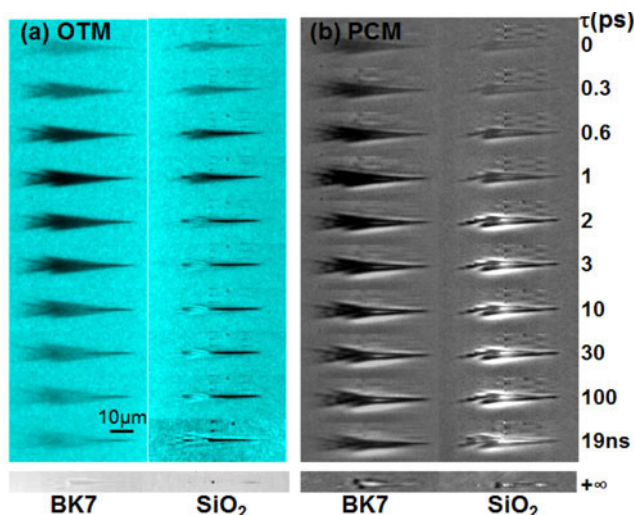


**Figure 4.** Time-resolved observation of excitation and relaxation in borosilicate BK7 and fused silica in (a) OTM and (b) PCM modes at energies moderately above the void-formation threshold. Input energy  $E = 4 \mu\text{J}$  and pulse duration  $t_p = 160 \text{ fs}$ . Two characteristic regions in terms of dynamics are visible with fast and slow carrier decay times, and specific structural arrangements accompanying the two dynamics. The differentiation in fast and slow decay times is particularly observable for a-SiO<sub>2</sub>, with a less pregnant distinction in the case of BK7.

difference in the carrier decay mechanisms, with probable deviations in the trapping dynamics due to the compositional and band structure changes. For the HF, the apparent longer decay for fused silica in this range is related to the specific thermodynamic trajectory assisting the transition to lower viscosity, while a thermomechanical scenario seems more probable for BK7 in view of its mechanical properties.

### 3.3. Mechanical relaxation

Even if the electronic concentration is quasi-sub-critical, in the catastrophic damage range the deposited energy can bypass the glass softening point. The long decay times suggest the achievement of low viscosity regions. In this range mechanical relaxation is expected via the release of pressure waves that reflect the geometry of the source<sup>[19, 31]</sup> and the pressure–temperature conditions in the excitation region. Shock relaxation, plastic yielding and elastic response can occur, reflecting the development of a hot, pressurized region<sup>[25]</sup>. The observations here do not allow observing the initial shell-like shock which is confined on sub-micrometer scales, but merely the elastic propagation. The PCM observations for a-SiO<sub>2</sub> and BK7 at relatively long delays (2.5 ns, respectively 2.9 ns) given in Figures 5(a) and 5(b) show the emergence of pressure traveling waves with a velocity of 6.3 km/s (for fused silica), close to the longitudinal speed of sound. The overall form in case of a-SiO<sub>2</sub> [Figure 5(a)] comprises spherical and cylindrical components related to the void-like confined and filament-like elongated regions in the permanent damage morphology [Figure 1(d)]. The BK7

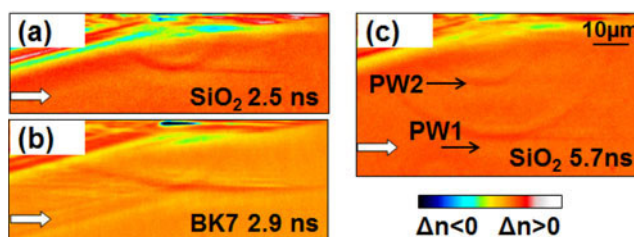


**Figure 5.** Long delay time (ns range) PCM observation of relaxation in (a) a-SiO<sub>2</sub> and (b) BK7 at energies significantly above the void-formation threshold (high-energy range). Input energy  $E = 43 \mu\text{J}$  and pulse duration  $t_p = 160 \text{ fs}$ . The color bar relates to evolving relative positive and negative refractive index changes. Pressure waves traveling at the speed of sound are to be observed as moving index change regions. (c) Longer delay time (5.7 ns) PCM observations in a-SiO<sub>2</sub> showing a second pressure wave forming with a delay of 2.7 ns. The laser pulse is coming from the left and the source is located at the top of each image.

case [Figure 5(b)] shows a more planar geometry reflecting the extended void-like damage in Figure 3(d). At longer delay times [Figure 5(c)] in the case of fused silica, a second pressure wave appears with a delay of 2.7 ns. If it appears to suggest mechanical rupture or fracture, the origin of these second waves remains unknown. A similar phenomenon was recently observed in soda-lime glass<sup>[32]</sup>.

The thermomechanical scenario is valid for a range of energies above the void-formation threshold inside the material and for a range of pulse durations. We follow below an example (illustrated in Figure 6) for observing the pressure waves initiated from the impact point in fused silica. The experimental detection concerns a moderate energy input of 4  $\mu\text{J}$  for an incident laser pulse of 2 ps duration and time-resolved phase-contrast imaging. Figure 6(a) describes experimentally the dynamics of the acoustic waves generated after the deposition of the laser pulse energy. The PCM observations concern several delay times in the ns domain and show the formation and evolution of spherical and cylindrical components of the pressure waves (circular and linear geometries in the 2D figure section). For simulation, the spatial energy deposition pattern for an 150 fs laser pulse is calculated using a nonlinear light propagation code<sup>[23]</sup> serving then as input for the calculus of acoustic wave fields<sup>[33]</sup> emerging from the hot source. The simulated dynamics of the acoustic propagation is given in Figure 6(b). Note that the laser-induced formation of permanent material damage and density redistribution is not included in the present photo-acoustic simulations, but elements of densification/rarefaction were previously discussed<sup>[34]</sup>. The spherical and plane components, the compression and unload waves as well as the asymmetrical character are well reproduced. In the first ns after the interaction, the geometry of the compression wave conserves the aspect of the heat source. Spherical waves are initiated at the two extremities of the focal trace and cylindrical waves are launched perpendicular to the elongated source. The asymmetry is given by a stronger localization of the energy before the focus due

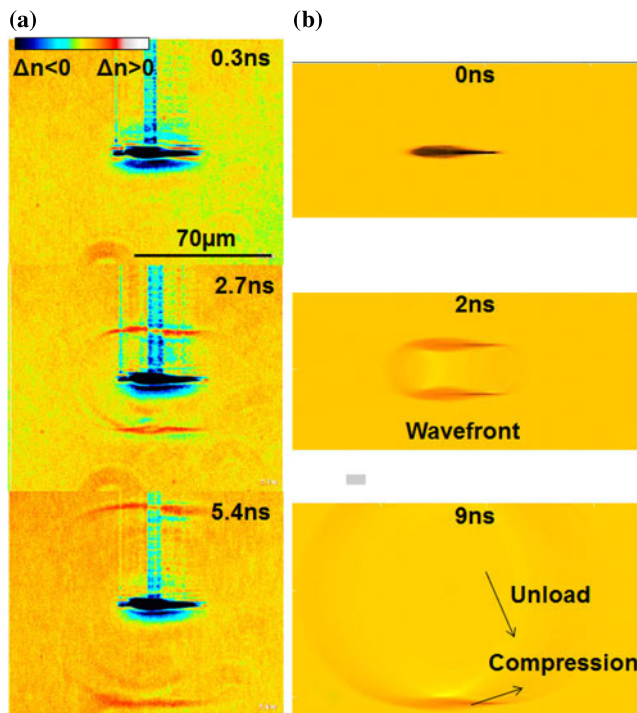


**Figure 6.** Photo-acoustic dynamics in fused silica observable at different time delays (a) in experimental time-resolved PCM images of evolving pressure waves and (b) in photo-acoustic simulation for a moderate energy input of  $4 \mu\text{J}$ . Pulse duration is 2 ps for (a) and 150 fs for (b). The laser pulse is coming from the left. The color bar relates to evolving relative positive and negative refractive index changes.

to self-focusing. An unload component develops, reflecting also the initial mapping of energy deposition.

### 3.4. Irradiation and control by temporally shaped pulses

The resulting modification at the level of the structure depends strongly on the ability to store energy into the glass matrix. Energy-dependent studies in the femtosecond range indicate that the local excitation does not vary significantly with the input intensity<sup>[23]</sup>, at least up to the point of uncontrollable, catastrophic damage. This is a direct consequence, at least for moderate focusing conditions, of the balance between pulse focusing strength including self-focusing and carrier defocusing, leading to a leveling of excitation similar to an intensity clamping effect. This leveling can be prevented by acting on the timing of the plasma formation<sup>[7]</sup> and on its radial distribution, notably using the pulse envelope and spectral dispersion as an adjustable parameter. The consequence is that by elongating pulse envelopes, to a certain extent counterintuitively, the amount of excitation increases, despite a reduction into multiphoton ionization cross-section. Figure 7 resumes this situation for an input energy of  $4 \mu\text{J}$  in fused silica, where the increase of pulse duration leads to a higher amount of energy

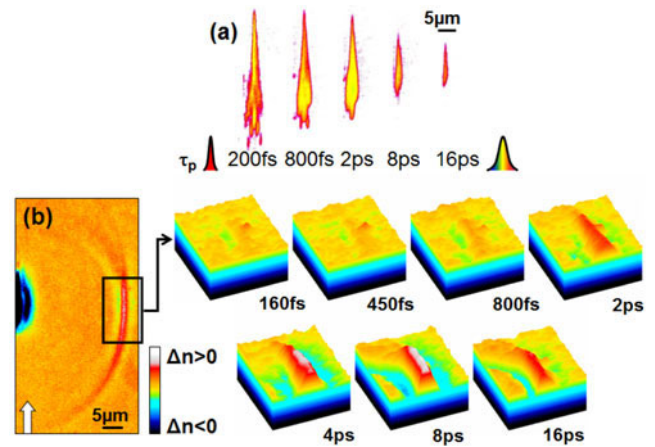


**Figure 7.** (a) Excitation increase (absorption maps in false colors) upon irradiation with pulses of increasing duration. (b) Pressure wave magnitude dependence in fused silica on the input pulse duration for an energy of  $4 \mu\text{J}$ . The color bar indicates relative positive and negative transient refractive index changes associated to thermomechanical phenomena.

concentration. This is first visible in the augmentation of the absorption level due to free carriers [Figure 7(a)], as well as in the subsequent increase in the magnitude of the launched pressure wave [Figure 7(b)]. A scenario discussing the role of pulse duration in defining the level and the shape of the absorption region was discussed earlier<sup>[7, 23]</sup>. The pulse durations that achieved the maximal carrier density and pressure yield respectively are slightly shifted, indicating that the released pressure only partially reflects the initial energy concentration, part of the energy being spent in plastic compaction around the damage region. Nevertheless, this shows that concepts of optimal interaction can be defined with respect to the energy deposition. We note that a similar behavior was observed for double pulse sequences with separation times comparable to the elongation of the long pulse (not shown).

## 4. Conclusions

In conclusion we have shown fast and slow characteristic dynamics of laser-excited free carriers in silica-based optical glasses, depending on the amount of excitation. If fast sub-ps decay is recognizable in a-SiO<sub>2</sub> for excitation levels at a fraction of the critical density, leading to carrier trapping and defect-based structural reorganization, slow dynamics signaling low viscosity states appears around the critical density. This is reflected in the damage morphology, from defect-induced densification to rarefaction, void-formation and mechanical compaction. Slower dynamics is observed for the borosilicate BK7 glass, suggesting qualitative changes in the decay mechanisms. Soft, carrier-driven and thermomechanically driven structural paths are recognizable and reflected in characteristic dynamics. In

thermomechanical ranges, mechanical relaxation via pressure release depends on the geometry and the magnitude of the heat source. Given the nonlinear propagation and energy feedthrough, optimization concepts for the energy deposition can be introduced based on pulse temporal tailoring.

### Acknowledgements

The authors thank P. K. Velpula and M. K. Bhuyan for their assistance. They equally acknowledge the financial support of the Agence Nationale de la Recherche (projects ANR 2011 BS04010 NanoFlam and ANR 2011 BS09026 SmartLasir).

### References

1. R. Osellame, G. Cerullo, and R. Ramponi, (Eds.) in *Femtosecond Laser Machining, Photonic and Microfluidic Devices in Transparent Materials*, Topics in Applied Physics (Springer, 2012).
2. W. Koechner, *Solid-state Laser Engineering*, Springer Series in Optical Sciences (Springer, 2006).
3. F. L. Galeener, D. L. Griscom, and M. J. Weber, (Eds.) in *Defects in Glasses* (Materials Research Society, 1986).
4. J. Ready, *Effects of High-Power Laser Radiation* (Academic Press, 1971).
5. P. N. Saeta and B. I. Greene, *Phys. Rev. Lett.* **70**, 3599 (1993).
6. P. Audebert, P. Daguzan, A. Dos Santos, J. C. Gauthier, S. Guizard, G. Hamoniaux, K. Krastev, P. Martin, G. Petite, and A. Antonetti, *Phys. Rev. Lett.* **73**, 1990 (1994).
7. P. K. Velpula, M. Bhuyan, F. Courvoisier, H. Zhang, J. P. Colombier, and R. Stoian, *Laser Photon. Rev.* **2**, 230 (2016).
8. Q. Sun, H. Jiang, Y. Liu, Z. Wu, H. Yang, and Q. Gong, *Opt. Lett.* **30**, 320 (2005).
9. A. Horn, E. W. Kreutz, and A. Poprawe, *Appl. Phys. A: Mater. Sci. Process.* **79**, 923 (2004).
10. D. G. Papazoglou, I. Zergioti, and S. Tzortzakis, *Opt. Lett.* **32**, 2055 (2007).
11. T. Balciunas, A. Melninkaitis, G. Tamosauskas, and V. Sirutkaitis, *Opt. Lett.* **33**, 58 (2008).
12. V. V. Temnov, K. Sokolowski-Tinten, P. Zhou, A. El-Khamhawy, and D. von der Linde, *Phys. Rev. Lett.* **97**, 237403 (2006).
13. I. H. Chowdhury, X. Xu, and A. M. Weiner, *Appl. Phys. Lett.* **86**, 151110 (2005).
14. D. Puerto, J. Siegel, W. Gawelda, M. Galvan-Sosa, L. Ehrentraut, J. Bonse, and J. Solis, *J. Opt. Soc. Am. B* **27**, 1065 (2010).
15. R. Stoian, M. Boyle, A. Thoss, A. Rosenfeld, G. Korn, I. V. Hertel, and E. E. B. Campbell, *Appl. Phys. Lett.* **80**, 353 (2002).
16. K. Mishchik, G. Cheng, G. Huo, I. M. Burakov, C. Maclair, A. Mermillod-Blondin, A. Rosenfeld, Y. Ouerdane, A. Boukenter, O. Parriaux, and R. Stoian, *Opt. Express* **18**, 24809 (2010).
17. P. G. Kazansky and Y. Shimotsuma, *J. Ceram. Soc. Japan* **116**, 1052 (2008).
18. A. Mermillod-Blondin, I. M. Burakov, Yu. P. Meshcheryakov, N. M. Bulgakova, E. Audouard, A. Rosenfeld, A. Husakou, I. V. Hertel, and R. Stoian, *Phys. Rev. B* **77**, 104205 (2008).
19. M. Sakakura, M. Terazima, Y. Shimotsuma, K. Miura, and K. Hirao, *J. Appl. Phys.* **109**, 023503 (2011).
20. M. Lancry, B. Poumellec, J. Canning, K. Cook, J.-C. Poulain, and F. Brisset, *Laser Photonics Rev.* **7**, 953 (2013).
21. A. Mermillod-Blondin, C. Maclair, J. Bonse, R. Stoian, E. Audouard, A. Rosenfeld, and I. V. Hertel, *Rev. Sci. Instrum.* **82**, 033703 (2011).
22. K. Mishchik, C. D'Amico, P. K. Velpula, C. Maclair, Y. Ouerdane, A. Boukenter, and R. Stoian, *J. Appl. Phys.* **114**, 133502 (2013).
23. I. M. Burakov, N. M. Bulgakova, R. Stoian, A. Mermillod-Blondin, E. Audouard, A. Rosenfeld, A. Husakou, and I. V. Hertel, *J. Appl. Phys.* **101**, 043506 (2007).
24. A. Mermillod-Blondin, J. Bonse, A. Rosenfeld, I. V. Hertel, Yu. P. Meshcheryakov, N. M. Bulgakova, E. Audouard, and R. Stoian, *Appl. Phys. Lett.* **94**, 041911 (2009).
25. E. G. Gamaly, S. Juodkasis, K. Nishimura, H. Misawa, B. Luther-Davies, L. Hallo, P. Nicolai, and V. T. Tikhonchuk, *Phys. Rev. B* **73**, 214101 (2006).
26. C. Maclair, A. Mermillod-Blondin, S. Landon, N. Huot, A. Rosenfeld, I. V. Hertel, E. Audouard, I. Myiamoto, and R. Stoian, *Opt. Lett.* **36**, 325 (2011).
27. D. Grojo, M. Gertssov, S. Lei, T. Barillot, D. M. Rayner, and P. B. Corkum, *Phys. Rev. B* **81**, 212301 (2010).
28. L. Bressel, D. de Ligny, E. G. Gamaly, A. V. Rode, and S. Juodkasis, *Opt. Mater. Express* **1**, 1150 (2011).
29. R. Stoian, K. Mishchik, G. Cheng, C. Maclair, C. D'Amico, J. P. Colombier, and M. Zamfirescu, *Opt. Mater. Express* **3**, 1755 (2013).
30. A. Mermillod-Blondin, 'Analysis and optimization of ultrafast laser-induced bulk modifications in dielectric materials', PhD Thesis (Free University Berlin and Jean Monnet University, 2007).
31. A. Salleo, F. Y. Génin, M. D. Feit, A. M. Rubenchik, T. Sands, S. S. Mao, and R. E. Russo, *Appl. Phys. Lett.* **78**, 2840 (2001).
32. F. Hendricks, V. V. Matylitsky, M. Domke, and H. P. Huber, *Proc. SPIE* **9740**, 97401A (2016).
33. B. E. Treeby and B. T. Cox, *J. Biomed. Opt.* **15**, 021314 (2010).
34. N. M. Bulgakova, *J. Appl. Phys.* **118**, 233108 (2015).